



HAL
open science

Mechanistic View and Genetic Control of DNA Recombination during Meiosis

Marie-Claude Marsolier-Kergoat, Md Muntaz Khan, Jonathan Schott, Xuan
Zhu, Bertrand Llorente

► **To cite this version:**

Marie-Claude Marsolier-Kergoat, Md Muntaz Khan, Jonathan Schott, Xuan Zhu, Bertrand Llorente.
Mechanistic View and Genetic Control of DNA Recombination during Meiosis. *Molecular Cell*, 2018,
70 (1), pp.9+. 10.1016/j.molcel.2018.02.032 . hal-02397018

HAL Id: hal-02397018

<https://amu.hal.science/hal-02397018v1>

Submitted on 23 Nov 2023

HAL is a multi-disciplinary open access archive for the deposit and dissemination of scientific research documents, whether they are published or not. The documents may come from teaching and research institutions in France or abroad, or from public or private research centers.

L'archive ouverte pluridisciplinaire **HAL**, est destinée au dépôt et à la diffusion de documents scientifiques de niveau recherche, publiés ou non, émanant des établissements d'enseignement et de recherche français ou étrangers, des laboratoires publics ou privés.

1 **Mechanistic view and genetic control of DNA recombination during meiosis**

2

3 Marie-Claude Marsolier-Kergoat^{1,2#*}, Md Muntaz Khan^{3#}, Jonathan Schott³, Xuan
4 Zhu^{4,5}, and Bertrand Llorente^{3,6*}

5

6

7 1. CEA/DRF, I2BC/UMR 9198, SBIGeM, 91191 Gif-sur-Yvette, France.

8 2. CNRS-UMR 7206, Éco-anthropologie et Ethnobiologie, Musée de l'Homme, 17,
9 place du Trocadéro et du 11 novembre, 75016 Paris, France.

10 3. Cancer Research Center of Marseille, CNRS UMR7258, Inserm U1068, Institut
11 Paoli-Calmettes, Aix-Marseille Université UM105, 13273 Marseille, France

12 4. Molecular Biology Program, Memorial Sloan Kettering Cancer Center and Howard
13 Hughes Medical Institute, New York, New York, United States of America

14 5. Present address : Baker Hughes, a GE company, San Ramon, California, USA

15 6. Lead contact

16 # These authors contributed equally to this work.

17 *Correspondence: mcmk@cea.fr (M.-C. M.-K.), bertrand.llorente@inserm.fr (B. L.)

18

19

20 **ABSTRACT**

21

22 Meiotic recombination is essential for fertility and allelic shuffling. Canonical
23 recombination models fail to capture the observed complexity of meiotic
24 recombinants. Here we revisit these models by analyzing meiotic heteroduplex DNA
25 tracts genome-wide in combination with meiotic DNA double-strand break (DSB)
26 locations. We provide unprecedented support to the synthesis-dependent strand
27 annealing model and establish estimates of its associated template switching
28 frequency and polymerase processivity. We show that resolution of double Holliday
29 junctions (dHJs) is biased toward cleavage of the pair of strands containing newly
30 synthesized DNA near the junctions. The suspected dHJ resolvase Mlh1-3 as well as
31 Mlh1-2, Exo1 and Sgs1 promote asymmetric positioning of crossover intermediates
32 relative to the initiating DSB and bidirectional conversions. Finally, we show that
33 crossover-biased dHJ resolution depends on Mlh1-3, Exo1, Msh5 and to a lesser
34 extent on Sgs1. These properties are likely conserved in eukaryotes containing the
35 ZMM proteins, which includes mammals.

36 INTRODUCTION

37

38 Decades of studies at a few loci in different organisms led to a global view of meiotic
39 recombination (Figure 1). In the representative *Saccharomyces cerevisiae* yeast
40 model, it starts by the formation of DNA double-strand breaks (DSBs) catalyzed by
41 the Spo11 topoisomerase II-like protein^{1,2}. Second, DNA ends are processed by the
42 Mre11-Rad50-Xrs2 complex and Sae2 to release Spo11 from the ends, which allows
43 Exo1 to further degrade the 5' ends and produce on average ca. 800 bp-long 3'
44 single-stranded DNA tails³⁻⁷. Third, a DNA tail invades a homologous template to
45 form a D-loop structure comprising a heteroduplex DNA (hDNA) plus a 3' end used to
46 prime DNA repair synthesis.

47 Next, under the synthesis-dependent strand annealing (SDSA) model, the
48 resected second end anneals to the newly synthesized DNA on the first end after D-
49 loop disruption to yield exclusively noncrossovers⁸⁻¹¹. The first hDNA formed is
50 transient but the second hDNA (newly synthesized DNA annealed to the second end)
51 may be present in the final noncrossover just 3' of the initiating DSB (Figure 1B and
52 2B).

53 Alternatively, under the canonical DSB repair model, the resected second end
54 anneals to the displaced strand of the D-loop, yielding an intermediate with two
55 Holliday junctions (dHJ). Depending on whether two or four DNA strands are
56 cleaved, dHJ resolution yields either a noncrossover or a crossover, respectively
57 (Figure 1C)^{4,12}.

58 While crossovers result from dHJ resolution, meiotic noncrossovers are
59 thought to mostly result from SDSA and dHJ dissolution by isomerization through
60 branch migration yielding trans hDNA tracts on the same chromatid (Figure 1B and

61 2D)¹³⁻¹⁵. In many organisms, including *S. cerevisiae*, plants, and mammals,
62 crossovers form through two distinct pathways. The major pathway relies on the
63 integrity of the synaptonemal complex and the resulting crossovers show
64 interference, *i.e.* they are more widely and evenly spaced than expected by chance.
65 In yeast, this ZMM pathway depends on Zip1, Zip2, Zip3, Zip4, Spo16, the Mer3
66 helicase and the heterodimer Msh4-Msh5 thought to protect recombination
67 intermediates from Sgs1-mediated dissolution^{16,17}. The heterodimeric endonuclease
68 Mlh1-Mlh3 in combination with Sgs1 and Exo1 are thought to constitute the
69 resolution machinery of the ZMM pathway¹⁸⁻²¹. The minor crossover pathway is
70 independent of the synaptonemal complex and the resulting crossovers do not show
71 interference²²⁻²⁴. It relies on the partially redundant structure-specific nucleases
72 Mus81-Mms4, Yen1 and Slx1-Slx4^{18,22,25,26}. Interestingly, dHJ resolution is biased
73 toward crossover in the ZMM pathway, but apparently not in the structure specific
74 nuclease pathway(s)^{18,27-30}. The mechanism for this bias is not known.

75 The hDNA tracts disposition in recombinants is key to understanding
76 recombination mechanisms. To be studied, they require either inactivation of
77 mismatch repair³¹ or poorly repairable substrates³². Under the canonical DSB repair
78 model, dHJ resolution yields hDNA tracts on both sides of the initiating DSB.
79 However, hDNA tracts were instead frequently observed on one side only^{13-15,33-36}
80 (Figure 3C). These one-sided events could reflect either a structural asymmetry of
81 the hDNA tracts formed early in the recombination reaction, or that some hDNA
82 tracts are transient.

83 Another prediction of the canonical model is that crossover-associated hDNA
84 should occur equally frequently in either of two configurations (patterns 1 and 2 in
85 Figure 1C), because both HJs should have equal likelihood of being resolved as a

86 crossover. However, a prevalence of crossovers occurring at the junction inferred to
87 result from the first strand invasion was observed, albeit to different extents among
88 the few loci analyzed^{33,34,37}. As this configuration requires cleavage of strands
89 proximal to the newly synthesized DNA tracts, it suggests that these tracts somehow
90 bias the orientation of HJ resolution.

91 Finally, the gain of genetic material at a recombination site is expected to be
92 unidirectional, from the intact donor to the broken recipient. However, bidirectional
93 exchanges of genetic information have been reported in many genetic studies
94 (Figure 3D and E), including those designed to follow recombination events arising
95 from a unique DSB hotspot³⁴. These were considered to be the result of multiple
96 independent Spo11-DSBs and were disregarded.

97 We recently developed a strategy to analyze meiotic hDNA genome-wide
98 from a S288C x SK1 hybrid lacking the Msh2 mismatch repair component (Figure
99 S1)¹⁵. Despite new insights provided, a major limitation was the lack of knowledge of
100 the location of the initiating DSBs, as for any other genome-wide study of
101 recombination so far. Therefore, here, we explore the discrepancies between
102 canonical models and *in vivo* recombination patterns by combining maps of genome-
103 wide Spo11-DSB locations with strand-transfer patterns in a mismatch repair-
104 defective reference strain and different recombination mutants. The results provide
105 unprecedented detail about global patterns and genetic control of recombination and
106 present a framework for revising and refining mechanistic recombination models.

107

108

109 RESULTS

110

111 Matching recombination events to initiating DSBs

112 Through sequencing Spo11-bound oligonucleotides (Spo11-oligos), we determined
113 the meiotic DSB map for the S288C x SK1 hybrid, which closely resembles that of
114 the SK1 x SK1 homozygote^{38,39}. In parallel we analyzed the progeny of four octads
115 derived from a diploid *msh2*Δ strain and inferred the most parsimonious scenarios for
116 the strand transfers characterizing recombination events⁴⁰. Figures 2A-H and 3A-I
117 show representative examples of the 367 noncrossovers and 448 crossovers
118 observed and listed in Table S1. In order to give a comprehensive and synthetic
119 description of these events, we coded them with series of colored segments (Figure
120 S2-5).

121 The Spo11-oligo map remarkably fits with the expected positions of initiating
122 DSBs for the recombination events (Figures 2A-H and 3A-H). To quantify the
123 goodness of this fit, the genome was divided into 50-bp segments and only the
124 segments harboring ≥ 16 associated Spo11-oligos were considered as DSB-
125 containing regions. Collectively, these DSB regions contain 95% of all Spo11-oligos
126 and cover 15% of the genome. We reasoned that for any set of recombination
127 events, 95% of the initiating DSBs should be located within these DSB regions (also
128 called "dsb95 segments") and we quantified the discrepancies between the expected
129 locations of DSBs inferred from the current recombination models and the positions
130 of the dsb95 segments for different kinds of events.

131

132

133 **DSB sites are found between noncrossover trans hDNA tracts, which supports**
134 **double SDSA and/or dHJ dissolution, and allows to infer strand orientation**

135 Noncrossovers characterized by two hDNA tracts in a trans configuration on the
136 same chromatid are expected to result either from double SDSA or from dHJ
137 dissolution (Figure 1B-C and 2D). This implies that a single Spo11-DSB initiates
138 them, and this DSB is necessarily 5' of the converted strands of the hDNA tracts. Our
139 observations support this hypothesis since we found that a DSB region overlaps the
140 region between the hDNA tracts in 53 out of 57 cases (#222-278) (Figure 2D and
141 S4), the remaining cases representing a fraction of events not significantly different
142 from the disregarded fraction of DSBs (p -value = 0.53, exact binomial test).
143 Consequently, we used such events to infer the orientation of the corresponding DNA
144 strands, a robust and critical piece of information not available from mere sequence
145 analysis (Figure S6).

146

147 **Both one-sided and two-sided noncrossovers support the SDSA pathway and**
148 **reveal a significant fraction of events associated with template switching**

149 After inference of strand orientation for 100 out of 185 SDSA-compatible events (#14-
150 198, Figure S4), we found that 85 oriented events contain a DSB region 5' of the
151 converted strands of the hDNA tracts (Figure 2B) as expected from the canonical
152 model. The 15 remaining events do not, which is statistically different from the
153 expected 5% of events arising from the disregarded fraction of DSBs (p = 0.00014,
154 exact binomial test). Unconverted SNPs between the presumed position of DSBs and
155 an SDSA hDNA tract can result from template switching, with the invading end first
156 engaging into the sister chromatid prior to engaging into the homolog (Figure 4A).
157 Following this hypothesis, we estimate that about 10 out of the 15 events correspond

158 to template switching, giving a probability of ~ 0.1 for a DNA end to switch template
159 when initiating SDSA. This calculation is an underestimate since we consider that a
160 causal DSB occurred at the expected location if this site overlaps a dsb95 region.
161 However, the causal DSB could occur at a different position in the dsb95 region that
162 could be compatible with template switching. In addition, template switching can take
163 place in regions devoid of markers and be undetectable.

164 Interestingly, among the 54 noncrossovers with trans hDNA tracts on the
165 same chromatid showing additional restoration and full-conversion tracts (#279-332,
166 Figure S4), 31 have a restoration patch exactly between the two hDNA tracts (#284-
167 314, Figures 2E and S4). The over-representation of restoration over full-conversion
168 patches and their biased location between the trans hDNA tracts support the
169 hypothesis that these events result from the double SDSA pathway. Indeed, initial
170 template switch between sister and non-sister chromatids automatically yields a
171 restoration patch between the trans hDNA tracts (Figure 4A). In contrast,
172 accumulation of nicks during dHJ dissolution followed by nick translation yields equal
173 proportions of restoration and full-conversion patches within the hDNA tracts but not
174 necessarily between the trans hDNA tracts (Figure 4B)¹⁵. Accordingly, comparing
175 these 31 noncrossovers with a single restoration patch exactly between the two
176 hDNA tracts with the 57 noncrossovers containing only two trans hDNA tracts (#222-
177 278, Figure S4) allowed us to propose that the proportion of DNA tails performing
178 template switching when initiating SDSA is likely higher than 0.2 (see Methods).

179 Overall, we bring unprecedented support to the SDSA model during meiosis.
180 Interestingly, our template switching estimate is close to the estimate of template
181 switching during break-induced replication in mitotic cells^{41,42}, a process sharing the
182 same initial steps with SDSA. The frequent interaction with the sister is rather

183 unexpected because of a strong homolog bias during meiotic recombination⁴³. Initial
184 invasion of the sister chromatid could be favored by the tight sister chromatid
185 cohesion mediated by Rec8 and later released by Red1/Mek1⁴⁴. Importantly, the
186 heteroduplex rejection property of the mismatch repair machinery that could promote
187 recombination with the sister chromatid is absent in our conditions⁴⁵. Therefore,
188 template switching likely reflects an intrinsic property of the recombination
189 mechanism that might be a consequence of the “collision release” process in which
190 pol delta ejects from PCNA upon extending a DNA template by running into a
191 downstream duplex⁴⁶. Such template switching was proposed to promote the
192 efficiency of the late steps of recombination¹⁷, and might also explain why most
193 noncrossovers-associated gene conversions in mice are away from the expected
194 DSB location^{47,48}.

195

196 **About one fifth of crossovers occur away from a mapped DSB region in events**
197 **with simple patterns**

198 The canonical DSB repair model predicts a strict connection between DSBs
199 and hDNA tracts associated to crossovers (Figures 1C and 3A-H). Remarkably, for
200 46 (11%) out of the 412 crossovers involving two non-sister chromatids, the
201 sequence located between the adjacent 4:4 segregating markers of the event (Figure
202 S2A) does not overlap a dsb95 segment (Figures 3I and S5). This is statistically
203 higher than the expected 5% (p -value = 6×10^{-7} , exact binomial test). This discrepancy
204 between expected and observed DSB locations reaches one out of five cases for
205 classes of crossovers with simple patterns where the expected DSB locations are
206 more restricted, *i.e.* crossovers with no associated strand transfer, crossovers with a
207 single full-conversion tract (#1-39, Figure S5), crossovers with a single hDNA tract

208 with or without an additional full-conversion tract (#63-116 and #135-156, Figures S5
209 and 3C) (see Methods). Several possibilities could account for this observation,
210 including template switching between sister and non-sister chromatids and HJ
211 mobility.

212

213 **Extensive HJ migration during DSB repair**

214 Out of 361 noncrossovers involving one or two non-sister chromatids, 29 (#333-361,
215 Figure S4) have strand transfer on two homologous chromatids, which is expected
216 from the resolution of a dHJ-containing intermediate (Figure 1C and 2H). Only two
217 exhibit the hDNA pattern expected from canonical dHJ resolution (#333-334), while
218 twenty contain symmetrical hDNA tracts. These tracts form either when a HJ
219 migrates within its adjacent homoduplex DNA, or when a DNA end performs template
220 switching engaging first into the sister chromatid prior to interacting with the homolog
221 (Figure 4C and D). The high frequency of symmetrical hDNA tracts and the
222 patchiness of the events that includes bidirectional conversion tracts (#353-361)
223 support the following model: nicks form during HJ branch migration potentially
224 through the abortive action of topoisomerases, and subsequent nick translation
225 results in patches of unidirectional or bidirectional conversions (Figure 4B and E)¹⁵.
226 HJ migration is also evidenced by noncrossovers #335-337 where inward migration
227 of one HJ with respect to the initiating DSB likely splits the original hDNA tract in two
228 pieces spread on the two recombining chromatids.

229 Likewise, many crossovers can be interpreted as exhibiting patterns
230 characteristic of HJ migration, including the 102 bidirectional crossovers (#240-341,
231 Figure 3D, F, J and S5), the 10 unidirectional crossovers with symmetrical hDNA
232 tracts, and a few other events containing trans hDNA tracts on one chromatid (for

233 example #199,200,204,223). In total, these crossovers represent at least 116 (28%)
234 events out of the 412 crossovers involving two chromatids. Finally, the significant
235 proportion of crossovers that do not exhibit a DSB region at the expected location
236 can result from HJ mobility (Figure 3I).

237 In conclusion, HJs frequently migrate during crossovers and noncrossovers
238 recombination. Although considered as a possibility by Szostak and colleagues¹², this
239 should now be included as a general feature of the DSB repair pathway and
240 considered when studying recombination events lengths.

241

242 **Meiotic phenotypes of mutants affecting the ZMM pathway at different steps**

243 The genetic control of the recombination patterns observed remains to be
244 determined. We therefore studied the *msh5* Δ mutant thought to block the ZMM
245 pathway early, the *mlh1* Δ , *mlh3* Δ , and *exo1* Δ mutants thought to block this pathway
246 at the resolution step, the meiotic null *pCLB2-SGS1* mutant expected to affect
247 several steps and pathways of recombination, and the *pms1* Δ and *mlh2* Δ mutants
248 whose corresponding proteins form two additional complexes with Mlh1. Full viable
249 *msh5* Δ octads could only be obtained in an *mlh2* Δ background^{40,49}.

250 Compared with the reference strain, we found a decrease in the number of
251 crossovers in the *mlh1* Δ , *mlh3* Δ , *exo1* Δ , and *mlh2* Δ *msh5* Δ mutants consistent with
252 previous reports^{3,50-52} (Figure 5A). This decrease seems more pronounced in the
253 *mlh3* Δ , *exo1* Δ and *mlh2* Δ *msh5* Δ mutants that also show chromosomes segregating
254 without crossovers (Table S1). The elevated number of noncrossovers in the *mlh2* Δ
255 *msh5* Δ mutant is reminiscent of a pairing defect known to prevent negative feedback
256 on DSB formation⁵³. Finally, we found that the lengths of the DNA strand transfers
257 associated to recombination events are increased to a similar extent in *mlh1* Δ and

258 *mlh2* Δ mutants, further supporting that the Mlh1-Mlh2 heterodimer is required to limit
259 hDNA tract extension⁴⁰ (Figure 5B).

260 The most remarkable changes in noncrossovers concern *pCLB2-SGS1*
261 (Figure 2C). The decrease in noncrossovers with trans hDNA tracts on one
262 chromatid could reflect impaired joint molecule dissolution⁵⁴⁻⁵⁶ and would explain at
263 least in part the increase in noncrossovers coming from dHJ resolution. The
264 unchanged fraction of SDSA compatible events could result from functional
265 redundancy with other helicases, such as Mph1 and Srs2⁵⁷. It could also suggest that
266 our strategy that relies on fully viable meiotic progeny is unable to reveal the
267 potentially more abundant branched intermediates in the absence of Sgs1^{17,58}, or that
268 the Sgs1 knock down is only partial in our condition⁵⁹.

269

270 **The apparent processivity parameter of the DNA repair polymerase involved in**
271 **the SDSA pathway is higher in the absence of Mlh1 or Mlh2**

272 In the absence of Msh2-dependent mismatch repair, hDNA tracts resulting from
273 SDSA correspond to tracts of newly synthesized DNA (Figure 1B). Since the
274 distributions of the lengths of hDNA tracts associated to SDSA-compatible events are
275 not statistically different for the reference and the *exo1* Δ strains (Figure 6), hDNA
276 tract lengths are likely determined by the new strand synthesis only and not by the
277 extent of Exo1-mediated resection^{60,61}. We therefore designed a strategy to extract
278 the apparent processivity parameter of the DNA repair polymerase at work during
279 SDSA (see Methods).

280 Briefly, we resorted to simulations to test different models of polymerase
281 activity. The choice of the distributions to model hDNA tracts lengths was guided by a
282 basic model of processive enzyme according to which the polymerase has a

283 probability p of moving to the next base and a probability $1-p$ of falling off. For the
284 reference strain, the best fit was obtained with $p = 0.9972$ (p -value = 0.52, chi-
285 squared test) (Figure 6). The quality of the fit supported our model.

286 The distributions of hDNA tracts lengths for the *exo1* Δ , *mlh3* Δ , *pms1* Δ , and
287 *pCLB2-SGS1* mutants were not different from that of the reference strain (p -value >
288 0.05, Fisher's test). In contrast, the distributions of hDNA tracts lengths for the *mlh1* Δ ,
289 *mlh2* Δ , and *mlh2* Δ *msh5* Δ mutants were significantly different from the reference (p -
290 value < 10^{-6}) with the best fits for p obtained with 0.9989 (p -value = 0.1), 0.9993 (p -
291 value = 0.8), and 0.9990 (p -value = 0.7), respectively. The distributions of hDNA
292 tracts lengths in the *mlh1* Δ , *mlh2* Δ , and *mlh2* Δ *msh5* Δ mutants can therefore be
293 accounted for by the simple model of a polymerase whose processivity is markedly
294 increased (0.9986-0.9994 compared to 0.9969-0.9977 for the reference strain).

295 Our data resemble the exponential relationship observed between the
296 frequencies of gene conversion and the distance from the DSBs, interpreted as
297 reflecting the processivity of a mismatch repair complex progressing from the DSB
298 site with a probability p of moving on to the next nucleotide. Data from the *ARG4*
299 locus led to a broad estimate of p between 0.9975 and 0.999 (for a review see⁶²).
300 However, comparison with our data is difficult since in an Msh2-dependent mismatch
301 repair-proficient context, conversion tracts are the end results of a series of
302 processes including DNA synthesis and mismatch repair of heteroduplexes that
303 could occur at several steps and lead either to conversion or restoration. Our *msh2* Δ
304 background constitutes a simpler system that allowed for the first time, to our
305 knowledge, to determine the apparent *in vivo* processivity parameter of a DNA repair
306 polymerase.

307

308 **Role of Mlh1-3 in the biased resolution of crossover-intermediates**

309 The two crossover resolution configurations can be distinguished depending
310 on whether the D-loop invading strand is cleaved or not (Figure 1C and S7, see
311 Methods). From the parsimonious analysis of four *msh2*Δ reference octads, 51 one-
312 sided and 27 two-sided crossovers showed a resolution pattern #1, and four one-
313 sided and zero two-sided crossovers showed a resolution pattern #2. The ratio of
314 crossovers with pattern #2 is significantly different from 0.5 in both cases (*p*-value
315 equal to 2.0×10^{-11} and 1.5×10^{-8} , respectively, exact binomial test), revealing a strong
316 bias toward resolution pattern #1 (Table 1). While such a bias was clearly established
317 during mitotic recombination in mammalian and yeast cells⁶³⁻⁶⁵, it was also detected
318 during yeast and fly meiosis at a few hot spots but with no definitive
319 conclusion^{33,34,37,66}. The nature of the signal associated with the newly synthesized
320 DNA is unknown, but an attractive hypothesis is that the nicks left after DNA repair
321 synthesis are not ligated prior resolution. Resolution of dHJs as crossovers would
322 therefore require only two additional nicks instead of four. This would also tend to
323 bias resolution toward crossovers versus noncrossovers, since noncrossover
324 resolution would require three nicks. Existence of nicked HJs was suggested from
325 electron microscopic observation of chromosomal DNA from pachytene yeast
326 cells^{23,67}, but is not supported by the work of Schwacha and Kleckner that observed a
327 majority of fully ligated joint molecules at the *HIS4-LEU2* hotspot⁴³. Remarkably, the
328 double-stranded DNA nicking activity of Mlh1-Mlh3 would allow resolution of nicked
329 HJs much better than of fully ligated HJs¹⁹⁻²¹.

330 We found that in all the mutants tested the proportion of two-sided crossovers
331 with pattern #2 over the total number of two-sided crossovers was not different from
332 that of the *msh2*Δ reference strain and that they all exhibit a clear bias in favor of

333 pattern #1 (Table 1). In contrast, we observed that the proportion of one-sided
334 crossovers with pattern #2 over the total number of one-sided crossovers was
335 significantly different from that of the reference strain for the *mlh3Δ* and *mlh1Δ*
336 mutants. This suggests that Mlh1-3 specifically promotes pattern #1 dHJ resolution of
337 one-sided crossover intermediates. Consequently, the alternative resolution pathway
338 mainly relying on Mus81 recognizes the imprints associated to the newly synthesized
339 DNA only for two-sided crossover intermediates. If these imprints are nicks, they
340 should be recognized and lead to crossover after Mus81 resolution^{68,69}). The
341 difference between one-sided and two-sided intermediates suggests that either such
342 nicks are lost in the absence of Mlh1-3 specifically for one-sided crossover
343 intermediates, or that the imprints are not nicks.

344

345 **Mlh1-3, Mlh1-2, Exo1 and Sgs1 promote one-sided crossovers with** 346 **bidirectional conversions and prevent accumulation of symmetrical hDNAs**

347 In the *mlh1Δ*, *mlh3Δ*, *exo1Δ*, *mlh2Δ*, *pCLB2-SGS1* and *mlh2Δ msh5Δ* mutants,
348 we found a global trend for crossover-associated strand transfers, that includes a
349 decrease in one-sided bidirectional gene conversions compared to the *msh2Δ*
350 reference strain, an increased frequency of two-sided crossovers and an increase in
351 symmetrical hDNA tracts (Figure 3J and S8).

352 Bidirectional gene conversions have always been considered as a result of
353 multiple initiating Spo11-DSBs in trans, normally repressed by Tel1 and Mec1⁷⁰.
354 Under this scenario, our observation would mean that Mlh1, Mlh2, Mlh3, Exo1 and
355 Sgs1 promote localized Spo11-DSBs in trans, although these proteins have no
356 known effect on Spo11 activity. Remarkably, bidirectional events mostly involve only
357 two chromatids, while a significant fraction of events involving at least three

358 chromatids would be expected if they resulted from multiple independent initiating
359 Spo11-DSBs. This leads to the alternative hypothesis postulated above where
360 bidirectional events would reflect Spo11-independent DNA breaks occurring during
361 the processing of recombination intermediates (Figure 4E). Mlh1-3, Mlh1-2, Exo1 and
362 Sgs1 would promote such processing, where the nuclease activity of Mlh1-3 could be
363 a source of nicks and even DSBs directly generating bidirectional conversions¹⁹⁻²¹.
364 The decrease in one-sided bidirectional conversions paralleled with the increase in
365 two-sided crossovers and crossovers with symmetrical hDNA tracts could suggest a
366 connection between these patterns controlled by Mlh1-3, Mlh1-2, Exo1 and Sgs1.
367 Importantly, this result combined with other recent results showing that Mlh1-2 limits
368 the extent of meiotic hDNA tracts⁴⁰ and that Mlh2 was lost concomitantly with Zip2, 3,
369 4, Spo16 and Msh4-5 in *Lachancea* yeasts⁷¹, reinforces the tight connection
370 between Mlh1-2 and the ZMM pathway.

371 Regarding two-sided crossovers, the *mlh1*Δ, *mlh3*Δ, *exo1*Δ and *pCLB2-SGS1*
372 mutants have more frequently trans hDNA tracts located on one chromatid rather
373 than on two recombining chromatids (Figure 3H, 5C). This pattern is reminiscent of
374 the resolution of a dHJ-containing intermediate after the migration of one HJ toward
375 the other HJ beyond the DSB site (Figure 4C)⁷². This result suggests that Mlh1,
376 Mlh3, Exo1 and Sgs1 limit inward HJ branch migration. Besides, the increase in
377 symmetrical hDNA tracts in their absence suggests that these four proteins also limit
378 outward HJ branch migration (Figure 5C). Accordingly, Sgs1 seems to prevent
379 branch migration under some circumstances, while this helicase is so far known to
380 undo joint molecules⁵⁴⁻⁵⁶. The polymer structure of Mlh1-3 might be important to limit
381 this Sgs1-independent HJ migration¹⁹. Moreover, these results support a possible
382 unanticipated role of Mlh1-3 before the resolution step⁵¹.

383 **Crossover resolution bias of dHJs**

384 Considering that noncrossovers involving two non-sister chromatids derive from dHJ
385 resolution, we could directly measure the crossover resolution bias of dHJs
386 previously identified²⁸⁻³⁰. We expressed it as 1 minus the ratio between
387 noncrossovers resulting from dHJ resolution and the total number of crossovers.
388 Compared to the *msh2Δ* reference, the bias is not affected in the *pms1Δ* nor *mlh2Δ*
389 mutants, but is significantly decreased in the *pCLB2-SGS1*, *mlh1Δ*, *mlh3Δ*, *exo1Δ*
390 and *mlh2Δ msh5Δ* mutants (Figure 5D). It is tempting to speculate that the crossover
391 bias could result from the dHJ resolution bias. However, the dHJ resolution bias is
392 always maintained for the two-sided crossover intermediates while the *exo1Δ*, *mlh1Δ*,
393 *mlh3Δ* and *mlh2Δ msh5Δ* mutants show a strong crossover bias defect. This shows
394 that the crossover bias and the dHJ resolution bias are independent, the crossover
395 bias being established prior to resolution.

396

397 **DISCUSSION**

398

399 The comprehensive analysis of meiotic hDNA from cells lacking the Msh2 mismatch
400 repair factor clarified our understanding of the mechanistic of meiotic recombination.
401 It revealed a remarkable and so far under appreciated dynamics of the meiotic DNA
402 transactions with frequent template switching and branch migration. It confirmed the
403 core of the DSB repair pathway, but identified variations from its canonical version.
404 The comparative analysis of different mutants notably revealed that Mlh1-3 promotes
405 both the asymmetric maturation and the biased resolution of crossover intermediates,
406 properties in line with its recent functional characterization^{19-21,50,51}. Given the

407 conservation of the proteins and pathways, we expect our findings apply to many
408 eukaryotes including mammals.

409

410 **AUTHOR CONTRIBUTIONS**

411

412 Conceptualization, MC.MK. and B.L.; Methodology, MM.K., MC.MK. and B.L.;
413 Software, MC.MK.; Formal Analysis, MC.MK. ; Investigation, MM.K., J.S., X.Z.,
414 MC.MK. and B.L.; Data Curation, MC.MK. and B.L.; Writing – Original Draft, MC.MK.
415 and B.L.; Supervision, MC.MK. and B.L.; Funding Acquisition, B.L.

416

417 **ACKNOWLEDGMENTS**

418

419 MCMK would like to thank Bruno Toupance (MNHN, Paris) for helpful discussions on
420 probability. We thank Scott Keeney for providing Spo11-oligo data, Olivier Espeli,
421 Romain Koszul and Mauro Modesti for discussions and Emmanuelle Martini and
422 Scott Keeney for critical reading of the manuscript. BL lab is funded by the ANR
423 (Agence nationale de la recherche) ANR-13-BSV6-0012-01 and ANR-16-CE12-
424 0028-01 grants. MMK is a recipient of a post doctoral fellowship from La Ligue
425 Contre le Cancer. JS was a recipient of a doctoral fellowship from La Ligue Contre le
426 Cancer. XZ was supported by National Institutes of Health grant R01 GM058673 (to
427 S. Keeney).

428

429

430 **REFERENCES**

431

- 432 1. Keeney, S., Giroux, C. N. & Kleckner, N. Meiosis-specific DNA double-strand
433 breaks are catalyzed by Spo11, a member of a widely conserved protein family.
434 *Cell* **88**, 375–384 (1997).
- 435 2. Sun, H., Treco, D., Schultes, N. P. & Szostak, J. W. Double-strand breaks at
436 an initiation site for meiotic gene conversion. *Nature* **338**, 87–90 (1989).
- 437 3. Zakharyevich, K. *et al.* Temporally and biochemically distinct activities of Exo1
438 during meiosis: double-strand break resection and resolution of double Holliday
439 junctions. *Mol. Cell* **40**, 1001–1015 (2010).
- 440 4. Sun, H., Treco, D. & Szostak, J. W. Extensive 3'-overhanging, single-stranded
441 DNA associated with the meiosis-specific double-strand breaks at the ARG4
442 recombination initiation site. *Cell* **64**, 1155–1161 (1991).
- 443 5. Mimitou, E. P., Yamada, S. & Keeney, S. A global view of meiotic double-
444 strand break end resection. *Science* **355**, 40–45 (2017).
- 445 6. Garcia, V., Phelps, S. E. L., Gray, S. & Neale, M. J. Bidirectional resection of
446 DNA double-strand breaks by Mre11 and Exo1. *Nature* 1–6 (2011).
447 doi:10.1038/nature10515
- 448 7. Neale, M. J., Pan, J. & Keeney, S. Endonucleolytic processing of covalent
449 protein-linked DNA double-strand breaks. *Nature* **436**, 1053–1057 (2005).
- 450 8. Nassif, N., Penney, J., Pal, S., Engels, W. R. & Gloor, G. B. Efficient copying of
451 nonhomologous sequences from ectopic sites via P-element-induced gap
452 repair. *Mol. Cell. Biol.* **14**, 1613–1625 (1994).
- 453 9. Ferguson, D. O. & Holloman, W. K. Recombinational repair of gaps in DNA is
454 asymmetric in *Ustilago maydis* and can be explained by a migrating D-loop

- 455 model. *Proc. Natl. Acad. Sci. U.S.A.* **93**, 5419–5424 (1996).
- 456 10. Pâques, F. & Haber, J. E. Multiple pathways of recombination induced by
457 double-strand breaks in *Saccharomyces cerevisiae*. *Microbiol. Mol. Biol. Rev.*
458 **63**, 349–404 (1999).
- 459 11. Resnick, M. A. The repair of double-strand breaks in DNA; a model involving
460 recombination. *J. Theor. Biol.* **59**, 97–106 (1976).
- 461 12. Szostak, J. W., Orr-Weaver, T. L., Rothstein, R. J. & Stahl, F. W. The double-
462 strand-break repair model for recombination. *Cell* **33**, 25–35 (1983).
- 463 13. Gilbertson, L. A. & Stahl, F. W. A test of the double-strand break repair model
464 for meiotic recombination in *Saccharomyces cerevisiae*. *Genetics* **144**, 27–41
465 (1996).
- 466 14. Porter, S. E., White, M. A. & Petes, T. D. Genetic evidence that the meiotic
467 recombination hotspot at the *HIS4* locus of *Saccharomyces cerevisiae* does
468 not represent a site for a symmetrically processed double-strand break.
469 *Genetics* **134**, 5–19 (1993).
- 470 15. Martini, E. *et al.* Genome-wide analysis of heteroduplex DNA in mismatch
471 repair-deficient yeast cells reveals novel properties of meiotic recombination
472 pathways. *PLoS Genet.* **7**, e1002305 (2011).
- 473 16. Lynn, A., Soucek, R. & Börner, G. V. ZMM proteins during meiosis: crossover
474 artists at work. *Chromosome Res.* **15**, 591–605 (2007).
- 475 17. Oh, S. D. *et al.* BLM Ortholog, Sgs1, Prevents Aberrant Crossing-over by
476 Suppressing Formation of Multichromatid Joint Molecules. *Cell* **130**, 259–272
477 (2007).
- 478 18. Zakharyevich, K., Tang, S., Ma, Y. & Hunter, N. Delineation of joint molecule
479 resolution pathways in meiosis identifies a crossover-specific resolvase. *Cell*

- 480 **149**, 334–347 (2012).
- 481 19. Manhart, C. M. *et al.* The mismatch repair and meiotic recombination
482 endonuclease Mlh1-Mlh3 is activated by polymer formation and can cleave
483 DNA substrates in trans. *PLoS Biol.* **15**, e2001164 (2017).
- 484 20. Ranjha, L., Anand, R. & Cejka, P. The *Saccharomyces cerevisiae* Mlh1-Mlh3
485 Heterodimer Is an Endonuclease That Preferentially Binds to Holliday
486 Junctions. *J. Biol. Chem.* **289**, 5674–5686 (2014).
- 487 21. Rogacheva, M. V. *et al.* Mlh1-Mlh3, A Meiotic Crossover and DNA Mismatch
488 Repair Factor, is a Msh2-Msh3-Stimulated Endonuclease. *J. Biol. Chem.*
489 (2014). doi:10.1074/jbc.M113.534644
- 490 22. de los Santos, T. *et al.* The Mus81/Mms4 endonuclease acts independently of
491 double-Holliday junction resolution to promote a distinct subset of crossovers
492 during meiosis in budding yeast. *Genetics* **164**, 81–94 (2003).
- 493 23. Stahl, F. W. *et al.* Does crossover interference count in *Saccharomyces*
494 *cerevisiae*? *Genetics* **168**, 35–48 (2004).
- 495 24. Zalevsky, J., MacQueen, A. J., Duffy, J. B., Kempfues, K. J. & Villeneuve, A. M.
496 Crossing over during *Caenorhabditis elegans* meiosis requires a conserved
497 MutS-based pathway that is partially dispensable in budding yeast. *Genetics*
498 **153**, 1271–1283 (1999).
- 499 25. De Muyt, A. *et al.* BLM Helicase Ortholog Sgs1 Is a Central Regulator of
500 Meiotic Recombination Intermediate Metabolism. *Mol. Cell* **46**, 43–53 (2012).
- 501 26. Matos, J., Blanco, M. G., Maslen, S., Skehel, J. M. & West, S. C. Regulatory
502 control of the resolution of DNA recombination intermediates during meiosis
503 and mitosis. *Cell* **147**, 158–172 (2011).
- 504 27. Oke, A., Anderson, C. M., Yam, P. & Fung, J. C. Controlling meiotic

- 505 recombinational repair - specifying the roles of ZMMs, Sgs1 and Mus81/Mms4
506 in crossover formation. *PLoS Genet.* **10**, e1004690 (2014).
- 507 28. Hunter, N. & Kleckner, N. The single-end invasion: an asymmetric intermediate
508 at the double-strand break to double-holliday junction transition of meiotic
509 recombination. *Cell* **106**, 59–70 (2001).
- 510 29. Allers, T. & Lichten, M. Differential timing and control of noncrossover and
511 crossover recombination during meiosis. *Cell* **106**, 47–57 (2001).
- 512 30. Börner, G. V., Kleckner, N. & Hunter, N. Crossover/noncrossover differentiation,
513 synaptonemal complex formation, and regulatory surveillance at the
514 leptotene/zygotene transition of meiosis. *Cell* **117**, 29–45 (2004).
- 515 31. Alani, E., Reenan, R. A. & Kolodner, R. D. Interaction between mismatch repair
516 and genetic recombination in *Saccharomyces cerevisiae*. *Genetics* **137**, 19–39
517 (1994).
- 518 32. Nag, D. K., White, M. A. & Petes, T. D. Palindromic sequences in heteroduplex
519 DNA inhibit mismatch repair in yeast. *Nature* **340**, 318–320 (1989).
- 520 33. Merker, J. D., Dominska, M. & Petes, T. D. Patterns of heteroduplex formation
521 associated with the initiation of meiotic recombination in the yeast
522 *Saccharomyces cerevisiae*. *Genetics* **165**, 47–63 (2003).
- 523 34. Jessop, L., Allers, T. & Lichten, M. Infrequent co-conversion of markers
524 flanking a meiotic recombination initiation site in *Saccharomyces cerevisiae*.
525 *Genetics* **169**, 1353–1367 (2005).
- 526 35. Allers, T. & Lichten, M. Intermediates of yeast meiotic recombination contain
527 heteroduplex DNA. *Mol. Cell* **8**, 225–231 (2001).
- 528 36. Hoffmann, E. R., Eriksson, E., Herbert, B. J. & Borts, R. H. MLH1 and MSH2
529 promote the symmetry of double-strand break repair events at the HIS4

- 530 hotspot in *Saccharomyces cerevisiae*. *Genetics* **169**, 1291–1303 (2005).
- 531 37. Foss, H. M., Hillers, K. J. & Stahl, F. W. The conversion gradient at HIS4 of
532 *Saccharomyces cerevisiae*. II. A role for mismatch repair directed by biased
533 resolution of the recombinational intermediate. *Genetics* **153**, 573–583 (1999).
- 534 38. Pan, J. *et al.* A Hierarchical Combination of Factors Shapes the Genome-wide
535 Topography of Yeast Meiotic Recombination Initiation. *Cell* **144**, 719–731
536 (2011).
- 537 39. Lam, I. & Keeney, S. Nonparadoxical evolutionary stability of the recombination
538 initiation landscape in yeast. *Science* **350**, 932–937 (2015).
- 539 40. Duroc, Y. *et al.* Concerted action of the MutL β heterodimer and Mer3 helicase
540 regulates the global extent of meiotic gene conversion. *eLife* **6**, (2017).
- 541 41. Smith, C. E., Llorente, B. & Symington, L. S. Template switching during break-
542 induced replication. *Nature* **447**, 102–105 (2007).
- 543 42. Llorente, B., Smith, C. E. & Symington, L. S. Break-induced replication: what is
544 it and what is it for? *Cell Cycle* **7**, 859–864 (2008).
- 545 43. Schwacha, A. & Kleckner, N. Identification of joint molecules that form
546 frequently between homologs but rarely between sister chromatids during
547 yeast meiosis. *Cell* **76**, 51–63 (1994).
- 548 44. Kim, K. P. *et al.* Sister cohesion and structural axis components mediate
549 homolog bias of meiotic recombination. *Cell* **143**, 924–937 (2010).
- 550 45. Chakraborty, U. & Alani, E. Understanding how mismatch repair proteins
551 participate in the repair/anti-recombination decision. *FEMS Yeast Research* **16**,
552 fow071 (2016).
- 553 46. Langston, L. D. & O'Donnell, M. DNA polymerase delta is highly processive
554 with proliferating cell nuclear antigen and undergoes collision release upon

- 555 completing DNA. *J. Biol. Chem.* **283**, 29522–29531 (2008).
- 556 47. Cole, F. *et al.* Mouse tetrad analysis provides insights into recombination
557 mechanisms and hotspot evolutionary dynamics. *Nature Publishing Group* **46**,
558 1072–1080 (2014).
- 559 48. Lange, J. *et al.* The Landscape of Mouse Meiotic Double-Strand Break
560 Formation, Processing, and Repair. *Cell* 1–21 (2016).
561 doi:10.1016/j.cell.2016.09.035
- 562 49. Abdullah, M. F. F., Hoffmann, E. R., Cotton, V. E. & Borts, R. H. A role for the
563 MutL homologue *MLH2* in controlling heteroduplex formation and in regulating
564 between two different crossover pathways in budding yeast. *Cytogenet.*
565 *Genome Res.* **107**, 180–190 (2004).
- 566 50. Al-Sweel, N. *et al.* mlh3 separation of function and endonuclease defective
567 mutants display an unexpected effect on meiotic recombination outcomes.
568 doi:10.1101/108498
- 569 51. Claeys Bouuaert, C. & Keeney, S. Distinct DNA-binding surfaces in the
570 ATPase and linker domains of MutL γ determine its substrate specificities and
571 exert separable functions in meiotic recombination and mismatch repair. *PLoS*
572 *Genet.* **13**, e1006722 (2017).
- 573 52. Wang, T. F., Kleckner, N. & Hunter, N. Functional specificity of MutL homologs
574 in yeast: evidence for three Mlh1-based heterocomplexes with distinct roles
575 during meiosis in recombination and mismatch correction. *Proc. Natl. Acad. Sci.*
576 *U.S.A.* **96**, 13914–13919 (1999).
- 577 53. Thacker, D., Mohibullah, N., Zhu, X. & Keeney, S. Homologue engagement
578 controls meiotic DNA break number and distribution. *Nature* **510**, 241–246
579 (2014).

- 580 54. Bachrati, C. Z. Mobile D-loops are a preferred substrate for the Bloom's
581 syndrome helicase. *Nucleic Acids Res.* **34**, 2269–2279 (2006).
- 582 55. Ira, G., Malkova, A., Liberi, G., Foiani, M. & Haber, J. E. Srs2 and Sgs1-Top3
583 suppress crossovers during double-strand break repair in yeast. *Cell* **115**, 401–
584 411 (2003).
- 585 56. Wu, L. & Hickson, I. D. The Bloom's syndrome helicase suppresses crossing
586 over during homologous recombination. *Nature* **426**, 870–874 (2003).
- 587 57. Mitchel, K., Lehner, K. & Jinks-Robertson, S. Heteroduplex DNA Position
588 Defines the Roles of the Sgs1, Srs2, and Mph1 Helicases in Promoting Distinct
589 Recombination Outcomes. *PLoS Genet.* **9**, e1003340 (2013).
- 590 58. Oh, S. D., Lao, J. P., Taylor, A. F., Smith, G. R. & Hunter, N. RecQ Helicase,
591 Sgs1, and XPF Family Endonuclease, Mus81-Mms4, Resolve Aberrant Joint
592 Molecules during Meiotic Recombination. *Mol. Cell* **31**, 324–336 (2008).
- 593 59. Kaur, H., De Muyt, A. & Lichten, M. Top3-Rmi1 DNA Single-Strand
594 Decatenase Is Integral to the Formation and Resolution of Meiotic
595 Recombination Intermediates. *Mol. Cell* **57**, 583–594 (2015).
- 596 60. Keelagher, R. E., Cotton, V. E., Goldman, A. S. H. & Borts, R. H. Separable
597 roles for Exonuclease I in meiotic DNA double-strand break repair. *DNA Repair*
598 (*Amst.*) **10**, 126–137 (2011).
- 599 61. Guo, X. & Jinks-Robertson, S. Roles of exonucleases and translesion
600 synthesis DNA polymerases during mitotic gap repair in yeast. *DNA Repair*
601 (*Amst.*) **12**, 1024–1030 (2013).
- 602 62. de Massy, B. Distribution of meiotic recombination sites. *Trends in Genetics* **19**,
603 514–522 (2003).
- 604 63. Baker, M. D. & Birmingham, E. C. Evidence for Biased Holliday Junction

- 605 Cleavage and Mismatch Repair Directed by Junction Cuts during Double-
606 Strand-Break Repair in Mammalian Cells. *Mol. Cell. Biol.* **21**, 3425–3435
607 (2001).
- 608 64. Mitchel, K., Zhang, H., Welz-Voegele, C. & Jinks-Robertson, S. Molecular
609 Structures of Crossover and Noncrossover Intermediates during Gap Repair in
610 Yeast: Implications for Recombination. *Mol. Cell* **38**, 211–222 (2010).
- 611 65. Yin, Y., Dominska, M., Yim, E. & Petes, T. D. High-resolution mapping of
612 heteroduplex DNA formed during UV-induced and spontaneous mitotic
613 recombination events in yeast. *eLife* **6**, (2017).
- 614 66. Crown, K. N., McMahan, S. & Sekelsky, J. Eliminating Both Canonical and
615 Short-Patch Mismatch Repair in *Drosophila melanogaster* Suggests a New
616 Meiotic Recombination Model. *PLoS Genet.* **10**, e1004583 (2014).
- 617 67. Bell, L. R. & Byers, B. Homologous association of chromosomal DNA during
618 yeast meiosis. *Cold Spring Harbor Symposia on Quantitative Biology* **47 Pt 2**,
619 829–840 (1983).
- 620 68. Osman, F., Dixon, J., Doe, C. L. & Whitby, M. C. Generating crossovers by
621 resolution of nicked Holliday junctions: a role for Mus81-Eme1 in meiosis. *Mol.*
622 *Cell* **12**, 761–774 (2003).
- 623 69. Dehé, P.-M. & Gaillard, P.-H. L. Control of structure-specific endonucleases to
624 maintain genome stability. *Nat. Rev. Mol. Cell Biol.* **18**, 315–330 (2017).
- 625 70. Zhang, L., Kleckner, N. E., Storlazzi, A. & Kim, K. P. Meiotic double-strand
626 breaks occur once per pair of (sister) chromatids and, via Mec1/ATR and
627 Tel1/ATM, once per quartet of chromatids. *Proc. Natl. Acad. Sci. U.S.A.* **108**,
628 20036–20041 (2011).
- 629 71. Vakirlis, N. *et al.* Reconstruction of ancestral chromosome architecture and

630 gene repertoire reveals principles of genome evolution in a model yeast genus.

631 *Genome Res.* (2016). doi:10.1101/gr.204420.116

632 72. Hoffmann, E. R. & Borts, R. H. Trans events associated with crossovers are

633 revealed in the absence of mismatch repair genes in *Saccharomyces*

634 *cerevisiae*. *Genetics* **169**, 1305–1310 (2005).

635

636

637

638 **FIGURE LEGENDS**

639

640 **Figure 1:** Canonical recombination pathways in the absence of mismatch repair. **a.**
641 Meiotic DSB processing. Homologous double-stranded DNA molecules are
642 represented by pairs of parallel blue and red lines. The arrowheads indicate the 5' to
643 3' polarity when needed. Dotted lines represent newly synthesized DNA. The left
644 product with no capture of the second end by the displaced strand of the D-loop is
645 channeled in the SDSA/double SDSA pathway (panel B). The right product is
646 channeled in the double Holliday junction processing pathway (panel C). **b.**
647 SDSA/double SDSA pathways. **c.** Processing of dHJs. Horizontal green arrows
648 indicate the direction of HJ branch migration during dissolution. Plain black
649 arrowheads represent the nick locations required for HJ resolution. There are two
650 resolution configurations for both noncrossovers and crossovers. The two end
651 products are identical for noncrossovers, but are distinct for crossovers. In pattern
652 #1, the hDNA tracts are in continuity with both parental duplexes, while they are in
653 discontinuity in pattern #2.

654

655 **Figure 2:** Examples and categorization of the noncrossovers detected in the *msh2Δ*
656 octads. **(a-h)** A representative set of noncrossovers involving one chromatid or two
657 non-sister chromatids. In the top part of each figure, vertical bars represent SNPs
658 locations, with the S288C and SK1 alleles as red and blue lines, respectively. Each
659 horizontal series of vertical bars is a DNA strand. One **(a-g)** or two **(h)** chromatids are
660 shown. The green lines represent the *dsb95* segments. The grey rectangles
661 correspond to the expected locations of the initiating DSBs according to the current
662 recombination models (see Figure 1). The bottom part of each figure shows the

663 counts of immunoprecipitated Spo11-FLAG oligos for each position, using S288C
664 coordinates. **a.** Noncrossover with a single full-conversion tract that is compatible
665 with gap repair. **b.** One-sided noncrossover with a half-conversion tract only. **c.** One-
666 sided noncrossover with a half-conversion tract and an internal patch of full
667 conversion. **d.** Two-sided noncrossover with two half-conversion tracts (trans hDNA)
668 affecting the same chromatid. **e.** Two-sided noncrossover with two half-conversion
669 tracts affecting the same chromatid and separated by a restoration tract. **f.** Two-sided
670 noncrossover with two half-conversion tracts affecting the same chromatid and
671 separated by a full-conversion tract. **g.** Two-sided noncrossover with two half-
672 conversion tracts affecting the same chromatid and an internal patch of full
673 conversion. **h.** Two-sided noncrossovers affecting two non-sister chromatids. **j.**
674 Noncrossovers categories. Noncrossovers were classified according to their strand
675 transfer pattern illustrated in panels **a-h** and the percentage of each category over
676 the total number of noncrossovers is shown. The stars indicate when the abundance
677 of the noncrossover category in a mutant is significantly different from the reference
678 *msh2Δ* strain (one star, $p < 0.05$; two stars, $p < 0.01$, Fisher's exact test).

679

680 **Figure 3:** Examples and categorization of the crossovers detected in the *msh2Δ*
681 octads. (**a-i**) A representative set of crossovers involving two non-sister chromatids
682 are schematized as in Figure 2. **a.** Crossover belonging to the category "no strand
683 transfer" in Figure 3J. **b.** Crossover with a single full-conversion tract. **c.** One-sided,
684 unidirectional crossover composed of a single half-conversion tract. **d.** One-sided,
685 bidirectional crossover. **e.** Two-sided, unidirectional crossover with trans hDNA tracts
686 on the two recombining chromatids. **f.** Two-sided, bidirectional crossover. **g.**
687 Crossover with a terminal tract of symmetrical hDNA possibly originating from HJ

688 branch migration. **h.** Two-sided, unidirectional crossover with trans hDNA tracts on
689 one chromatid only. **i.** Crossover belonging to the category "no strand transfer"
690 without any dsb95 segment located at the position expected for the causal DSB. **j.**
691 Crossover categories. Crossovers were classified according to their strand transfer
692 pattern (see panels **a-i**) and the percentage of each category over the total number of
693 crossovers is shown. The first seven categories are mutually exclusive. The stars
694 indicate when the abundance of the crossover category in a mutant is significantly
695 different from the reference *msh2Δ* strain (one star, $p < 0.05$; two stars, $p < 0.01$,
696 Fisher's exact test).

697
698 **Figure 4:** Variations from the canonical noncrossover and crossover formation
699 pathways. **a.** The outcome of SDSA is a half-conversion tract located exactly 3' of the
700 invading end on the broken chromatid. In case of initial invasion of the sister
701 chromatid prior to a switch to a non-sister chromatid, the half-conversion tract is
702 separated from the 3' invading end by a restoration tract. During single SDSA, this
703 can result in the presence of unconverted SNPs between the DSB site and the half-
704 conversion tract. During double SDSA, this automatically yields a restoration tract
705 between two trans hDNA tracts. **b.** Nick translation during dHJ dissolution can also
706 generate restoration tracts between trans hDNA tracts (left). However, depending on
707 the location of the nick, nick translation can result in either restoration or full
708 conversion, anywhere along the two trans hDNA tracts (middle and right). **c.** Branch
709 migration and crossover resolution. Branch migration (green arrows) of crossover
710 intermediates affects the strand transfer patterns of the recombination outcomes.
711 Left. D-loop migration erases the hDNA tract composed of the invading 3' end. Only
712 one hDNA tract positioned on the left side of the initiating DSB is present in the final

713 “one-sided” crossover. Middle. Branch migration of a single HJ away from the
714 initiating DSB within a homoduplex DNA region generates symmetrical hDNA tracts
715 (bracketed region). Right. Branch migration of the two HJ in the same direction can
716 position the two hDNA tracts on the same chromatid while they were initially on the
717 two recombining chromatids. Note that in case of noncrossover resolution, this
718 generates trans hDNA tracts indistinguishable from those resulting from double
719 SDSA or dHJ dissolution. In addition, in case of a long enough branch migration, a
720 restoration tract can be formed between the hDNA tracts and the crossover site
721 (bracketed region). Finally, symmetrical hDNA tracts corresponding to the region
722 between the two HJs can also form. **d.** Template switching and crossover resolution.
723 Invasion and DNA repair synthesis from a sister chromatid of one of the two 3’ ends
724 prior to interacting with the displaced strand of the D-loop formed with the
725 homologous chromatid by the other 3’ end generates a patch of symmetrical hDNA.
726 This patch of symmetrical hDNA is flanked either by two hDNA tracts if there is DNA
727 synthesis from the non-sister chromatid after template switch (left), or by a single
728 hDNA tract in the absence of DNA repair synthesis from the non-sister chromatid
729 (right). **e.** Nick translation within symmetrical hDNA tracts yields patchy unidirectional
730 and bidirectional conversions.

731
732 **Figure 5:** Meiotic characteristics of the strains used. **a.** Mean number of crossovers
733 and noncrossovers per octad. **b.** Median length of the strand transfers associated
734 with crossovers and noncrossovers. The length is defined as the distance between
735 the midpoints of the intermarker intervals surrounding the recombination event. Stars
736 indicate when the lengths are significantly different in the mutant and in the reference
737 *msh2Δ* strain (one star, $p < 0.05$; two stars, $p < 0.01$, Wilcoxon test). For clarity

738 reasons, the variability of the events lengths is not represented here but can be
739 computed from Table S1. **c.** Two-sided crossovers subcategories. Percentage of
740 two-sided crossovers with at least one pair of trans hDNA tracts on one chromatid.
741 The stars indicate when the ratios are significantly different in the mutant and in the
742 reference *msh2Δ* strain (one star, p -value < 0.05; two stars, p -value < 0.01, Fisher's
743 exact test). The numbers of events considered are 49, 33, 51, 24, 45, 28, 29 and 72
744 for the reference strain and the *pms1Δ*, *mlh1Δ*, *mlh3Δ*, *mlh2Δ*, *mlh2Δ msh5Δ*, *exo1Δ*
745 and *sgs1* mutants, respectively. **d.** Crossover bias. Crossover bias corresponds to 1
746 minus the ratio between the noncrossovers derived from resolution and the total
747 number of crossovers. Stars indicate when the crossover bias is significantly different
748 from the reference *msh2Δ* strain (one star, p < 0.05; two stars, p < 0.01, Fisher's
749 exact test). The numbers of events considered are 470, 281, 165, 111, 189, 120, 117
750 and 257 for the reference strain and the *pms1Δ*, *mlh1Δ*, *mlh3Δ*, *mlh2Δ*, *mlh2Δ*
751 *msh5Δ*, *exo1Δ* and *sgs1* mutants, respectively.

752
753 **Figure 6:** Distributions of hDNA tract lengths for the reference strain and several
754 mutants. hDNA length corresponds here to *len_mid* values, defined as the distance
755 between the midpoints of the intermarker intervals adjacent to the hDNA tract. The
756 red histograms represent the distributions of the observed *len_mid* values divided
757 into 100 bp bins. For each strain, the density functions of the simulation sets for the
758 processivity value p giving the best fit to the observed distribution are shown as
759 black, thin lines whereas the thick, green line represents the average of these density
760 functions. The numbers of data values are 247, 123, 117, 84, and 220, for the
761 reference strain and the *exo1Δ*, *mlh1Δ*, *mlh2Δ*, and *mlh2Δ msh5Δ* mutants,
762 respectively. Some extreme *len_mid* values are not represented on the graphs,

763 namely 4510, 4841, and 5052 for the *mlh1* Δ mutant, 4220, 4504, 4750, 5048, and
764 7300 for the *mlh2* Δ mutant, and 4480, 4708, 5730, 6794, 7330, and 8884 for the
765 *mlh2* Δ *msh5* Δ mutant.

766

767

768 **MATERIALS AND METHODS**
769

770 **Strains and media**

771 All yeast strains used in this study are derivatives of S288C⁷³ and SK1⁷⁴. Strain
772 genotypes are listed in Table S2. Gene disruptions were performed by PCR-
773 mediated gene replacement⁷⁵ followed by PCR analysis for discriminating correct
774 and incorrect gene targeting. S288C x SK1 crosses were made on YPD plates and
775 diploids were subcloned onto selective plates before transfer on 1% potassium
776 acetate sporulation medium and subsequent dissection. The hybrids made for octad
777 sequencing are BLY-HY1 to 8 (Table S2). Note that the octad datasets for *msh2Δ*
778 (BLY-HY1) and *msh2Δ mlh2Δ* (BLY-HY5) are the same as in⁴⁰.

779

780 **Spo11-oligo mapping**

781 A previously described, fully functional FLAG-tagged version of Spo11 was used^{53,76}.
782 The starting S288C strain was strain YTT0559 from the T. Tsukiyama lab, Fred
783 Hutchinson Cancer Research Center and was generously provided by I. Whitehouse,
784 Memorial Sloan Kettering Cancer Center. The endogenous *SPO11* locus in this
785 strain was tagged by integration of a *6His-3FLAG-loxP-kanMX-loxP* construct
786 amplified from an SK1 strain provided by Kunihiro Ohta, Univ. of Tokyo⁷⁶, creating
787 SKY4300. Correct tagging was verified by PCR and Southern blot. The SK1 parent
788 (SKY4301) was derived from standard SK1 strains in the S. Keeney laboratory
789 (Memorial Sloan Kettering Cancer Center) and has a series of single-base changes
790 introduced within and near the DSB hotspots in the *PDR3*, *RIM15*, *CCT6*, and *IMD3*
791 promoters; these base changes do not detectably alter the DSB distribution as
792 assessed by Spo11-oligo mapping (X. Zhu, S. Globus, and S. Keeney, unpublished

793 observations). SKY4300 and SKY4301 were mated to generate the F1 hybrid diploid
794 strain (SKY4302) used for Spo11-oligo mapping.
795 Spo11-oligo mapping was performed as previously described^{77,78} except that meiotic
796 cultures from SKY4302 were harvested 6 hr after transfer to sporulation medium.
797 Briefly, Spo11 oligos were purified by immunoprecipitation with anti-FLAG antibodies,
798 then sequencing adapters were added and the oligos were amplified by PCR and
799 sequenced. Sequencing was performed using Illumina HiSeq in the Memorial Sloan
800 Kettering Cancer Center Integrated Genomics Operation core facility. *In silico*
801 clipping of sequencing adapters and mapping of reads to the sacCer2 genome
802 assembly was performed using a previously described custom pipeline⁵³. After
803 mapping, the reads were separated into unique and multiple mapping sets, but only
804 uniquely mapping reads were used in this study (multiple mapping reads constituted
805 a small minority of the total). In Figures 2-3 and S6, the absolute number of uniquely
806 mapping Spo11-oligos is shown for each position.

807

808 **DNA extraction and octad sequencing**

809 To determine the meiotic strand transfers that occurred in the absence of Msh2, we
810 systematically generated and genotyped octads from S288C x SK1 hybrids. As
811 described in Figure S1, octads were obtained by inducing sporulation of such hybrids
812 and separating the mother from the daughter cells after the first mitotic division of the
813 four viable spores. Genomic DNA was purified from overnight saturated YPD culture
814 using a Qiagen genomic-tip 100/G. Sequencing was performed at BGI using Illumina
815 HiSeq instruments. We analyzed four octads from the *msh2* Δ hybrid, three from the
816 *msh2* Δ *pms1* Δ hybrid and two from all the other hybrids. For each genetic

817 background, all the recombination events from all the octads sequenced were pooled
818 for analysis.

819

820 **Genotyping and recombination event calling**

821 Spores were sequenced to an average sequencing depth of 50-60x. The reads were
822 aligned on the reference sequences of the parental strains S288C and SK1 using the
823 BWA software⁷⁹. We used the sequences from the *Saccharomyces* Genome
824 Database (SGD) web site (<http://www.yeastgenome.org/>) for S288C and the
825 sequence made available by S. Keeney (http://cbio.mskcc.org/public/SK1_MvO/) for
826 SK1. Only the reads matching perfectly the reference sequences were taken into
827 account. S288C-SK1 genome alignment was performed using the LAGAN
828 software⁸⁰. Only the aligned blocks longer than 2 kb were taken into account and
829 within these blocks only single nucleotide polymorphisms (SNPs) were considered.
830 The parental strains used in this study were also sequenced and all positions whose
831 base identity was not confirmed were eliminated. Finally, SNPs located in repeated
832 regions, long terminal repeats (LTRs), retrotransposons and telomeres were
833 discarded, which yielded a final list of 74,911 SNPs.

834 Genotyping was performed using stringent criteria: for a given SNP position, if
835 reads matched only one parental sequence, at least 15 reads were required, but if
836 reads aligned to both parental sequences, less than 5 reads matching one parental
837 sequence and at least 40 reads matching the other parental sequence were required
838 for base identity to be confirmed. Chromosomes were then segmented into stretches
839 of SNPs with identical genotypic patterns. These patterns are coded as x:y with x
840 representing the number of S288C alleles and $y = 8-x$ representing the number of
841 SK1 alleles. Accordingly, a 4:4 segment corresponds to a Mendelian segregation

842 profile, 5:3 and 3:5 segments to half-conversion tracts, 6:2 and 2:6 segments to full-
843 conversion tracts, etc.

844 We defined a recombination event as a set of adjacent segments located
845 between two 4:4 segments longer than 1.5 kb (the length used here is the distance
846 between the midpoints of the intermarker intervals adjacent to the segment). It has to
847 be noted that one recombination event can contain zero, one or two crossovers.
848 Figure 5A gives the total number of crossovers present in the events (counting two
849 crossovers for the few events concerned). In the rest of the article "crossover" refers
850 to "a recombination event including at least one crossover". The events were
851 classified as a function of the number of chromatids involved: one chromatid, two
852 chromatids, either sister or non-sister, and more than two chromatids. Only events
853 affecting one chromatid or two non-sister chromatids are represented in Figures 2, 3,
854 S4 and S5.

855 Overall, we tried to come up with the most parsimonious explanation for the strand
856 transfer tracts observed at recombination events. The complexity of strand transfer
857 tracts includes restoration patches, full-conversion patches and bidirectional
858 conversions. A simple scenario to explain restoration and full-conversion patches
859 consists of invoking an Msh2-independent short-patch mismatch repair pathway⁸¹
860 but there is no evidence in *S. cerevisiae* that such a pathway exists independently of
861 recombination. Accordingly, throughout the paper and when possible, we tried to
862 propose more parsimonious recombination-linked mechanisms to explain these
863 patches, whose occurrence would be independent from mismatch repair processes.
864 For instance, restoration tracts are compatible with template switch between the
865 sister and the non-sister chromatids (Figure 4A) and full conversions can be the
866 scars of gap repair (Figure S9). We also propose that restorations, full conversions

867 and bidirectional conversions could result from a nick translation process, initiated at
868 nicks that would form during the processing of recombination intermediates¹⁵ (Figure
869 4B and 4E). These nicks could result from aborted actions of SSNs or
870 topoisomerases such as Top3 during HJ branch migration, but also from Mlh1-3 that
871 can even generate DSBs¹⁹. Finally, some of the full conversions observed might also
872 derive from the mismatch repair-independent action of the proof-reading activity of
873 polymerase delta⁸².

874

875 **Estimating the frequency of initial template switching in the SDSA pathway**

876 The frequency of initial template switching between sister and non-sister chromatids
877 during SDSA can be estimated by comparing the 31 noncrossovers with a single
878 restoration patch exactly between the two hDNA tracts (that likely derive from double
879 SDSA with at least one of the DNA ends performing template switching) with the 57
880 noncrossovers containing only two trans hDNA tracts (#222-278, Figure S4). If these
881 57 noncrossovers all derive from dHJ dissolution, and none from double SDSA, we
882 get a probability of 1 for the DNA ends to perform template switching when initiating
883 SDSA. Conversely, if these 57 noncrossovers all derive from double SDSA, we can
884 calculate the probability p of initial template switching by one of the DNA ends when
885 initiating SDSA as follows. The proportion of SDSA events without template
886 switching, $57/(57+31)$, corresponds to the probability that none of the two DNA ends
887 will perform template switching, that is $(1-p)(1-p)$. From this, we can extract the value
888 of $p = 0.20$. Because of the probable existence of undetected central restoration
889 patches, this calculation yields an underestimate of p , so we propose that the
890 proportion of DNA tails performing template switching when initiating SDSA is likely
891 higher than 0.2.

892

893 **Comparing expected and observed DSB locations for crossovers with simple**
894 **patterns**

895 We consider classes of crossovers with simple patterns, for which the DSB locations
896 that are expected under the standard recombination models are restricted to one
897 segment or even one intermarker interval. There are no overlaps between DSB
898 regions (dsb95 segments) and event sectors for 16 (23%) out of 71 crossovers with
899 no associated strand transfer (Figure 3A and I), nor for 7 (18%) out of 39 crossovers
900 with a single full-conversion tract (#1-39, Figure S5 and 3B) that are compatible with
901 gap repair. In both cases, the ratios are statistically different from the expected 5%
902 (p -values equal to 4×10^{-7} and 3×10^{-3} , respectively). For some events, determining
903 chromatid orientation allows to define more precisely the expected location of DSB.
904 We were able to infer chromatid orientation for 55 events among 54 crossovers with
905 a single hDNA tract (#63-116, Figures S5 and 3C) and 22 crossovers consisting of a
906 single full-conversion tract and a single hDNA tract (#135-156, Figure S5). No DSB
907 region was present at the expected location in 13 (24%) cases out of these 55
908 oriented crossovers (p -value = 2×10^{-6}).

909

910 **Estimating the apparent processivity parameter of the DNA repair polymerase**
911 **involved in the SDSA pathway**

912 Several options are available for determining the mechanistic parameters of the DNA
913 repair polymerase involved in the SDSA pathway. A first option is to try to extract
914 from the markers positions of each event an estimate of the actual length of the
915 hDNA tract that includes the newly-synthesized DNA strand. The parameter len_{mid} ,
916 corresponding to the distance between the midpoints of the intermarker intervals

917 adjacent to the hDNA tract, is often used as such an estimate. However this estimate
918 exhibits several short-comings. First, it tends to be artificially inflated for short hDNA
919 tracts. Second, the value of *len_mid* crucially depends on the local density of
920 markers. Since the markers density widely fluctuates along the genome and could be
921 biased relative to the positions of the Spo11-DSB hotspots, it is difficult to find a
922 model allowing to extract from *len_mid* an adjusted estimate of the actual hDNA
923 lengths.

924 We therefore resorted to simulations for testing models of the polymerase
925 activity by comparing the distributions of observed and simulated *len_mid* values. We
926 calculated the *len_mid* values of two sets of noncrossovers enriched in SDSA events:
927 the noncrossovers comprising a single hDNA tract that we consider most likely
928 derived from the single SDSA pathway (#14-198, Figures 1B, 2B and S4 for the
929 reference strain) and the noncrossovers with a restoration patch exactly between two
930 trans hDNA tracts that we consider as probably originating from the double SDSA
931 pathway (#284-314, Figures 4A, 2E and S4 for the reference strain). In all cases, for
932 a given strain, the distributions of the *len_mid* values of the two sets of
933 noncrossovers were not statistically different and all *len_mid* values were therefore
934 pooled together.

935 We considered the simplest model of a processive enzyme with a probability p
936 of moving to the next base and a probability $1-p$ of falling off. Sets of 1,000 DSB
937 positions were sampled across the genome, weighting each position by its frequency
938 of Spo11-DSBs, as determined by the counts of immunoprecipitated Spo11-FLAG
939 oligos. Random values of hDNA lengths were generated from exponential
940 distributions of parameter $1-p$. Different ranges of values were tested for p ,
941 depending on the strains. For each value of p , independent sets of 1,000 simulated

942 *len_mid* values were generated. From the genomic boundaries of the simulated
943 hDNAs (associating a sampled DSB position and a random value of hDNA length)
944 and the positions of the local markers, we determined *len_mid* values. The
945 distribution of the observed *len_mid* values was then compared to the average
946 density function of five independent sets of simulated *len_mid* values, using
947 Pearson's chi-squared test. Considering only the values of p for which the p -value for
948 Pearson's goodness-of-fit test was higher than 0.1, we could estimate the
949 processivity of the repair polymerase between 0.9969 to 0.9977 for the reference
950 strain, between 0.9971 and 0.9982 for the *exo1* Δ mutant, between 0.9990 and
951 0.9994 for the *mlh2* Δ mutant and between 0.9986 and 0.9991 for the *mlh2* Δ *msh5* Δ
952 mutant.

953 Finally we found that for the reference strain the distribution of the lengths of
954 the 114 hDNA tracts associated to the 57 noncrossovers composed of two trans
955 hDNA tracts on the same chromatid (#222-278, Figures 2D and S4) was not
956 statistically different from that of the single SDSA-compatible events (p -value = 0.62,
957 Fisher's test). This suggests either that the noncrossovers with two trans hDNAs on
958 the same chromatid derives mostly from double SDSA or, if these noncrossovers
959 derive from dHJ dissolution, that the processivity of the polymerase operating in this
960 second pathway is similar to that of the polymerase operating during SDSA.

961

962 **Chromatid strand orientation**

963 The reconstruction of the sequences of the two DNA strands of each chromatid in a
964 given tetrad by sequencing the eight genomes of the corresponding octad does not
965 allow to infer the strand orientation of the chromatids from the tetrad (Figure S1). To
966 extract chromatid strand orientation, we performed several steps using recombination

967 events with patterns of increasing complexity. In a first step, we used noncrossovers
968 involving only one chromatid and including trans hDNA tracts, either adjacent or
969 separated by a single restoration or full-conversion tract. Chromatid orientation could
970 be automatically inferred from these events since the initiating DSB is expected to be
971 located 5' of the converted strand of the hDNA tracts (Figure 1B). In a second step,
972 chromatid orientation was manually derived from the analysis of crossovers and
973 noncrossovers involving two non-sister chromatids and including trans hDNA tracts,
974 either adjacent or separated by a single restoration or full-conversion tract, in addition
975 to crossovers containing only one half-conversion tract and one full-conversion tract
976 (that correspond presumably to gap repair (Figure S7)). At that stage strand
977 orientation determination benefited from the information gathered at the first step and
978 from the Spo11-oligo-based DSB map. Finally, crossovers and noncrossovers
979 containing symmetrical hDNA tracts were used to automatically complete chromatid
980 orientation since in these cases the strand orientation of one chromatid allows to infer
981 the strand orientation of the other chromatid involved. For each octad, 4 x 16
982 chromatids had to be oriented. In many cases, chromatid orientation could be
983 deduced from different events and we systematically checked the consistency of
984 these inferences (Figure S6). For example, for the first octad of the reference strain,
985 the orientation of 29 chromatids was determined more than once, and all multiple
986 orientations were consistent. In other cases, events involving one of the few
987 chromatids with inconsistent orientations were disregarded.

988 Chromatid orientation was used (i) for deducing the expected location of DSB
989 regions for one-sided crossovers and noncrossovers, *i.e.* the 5' end of the converted
990 strand of the hDNA tract, and (ii) for determining the resolution pattern of crossovers.
991

992

993 **Determining the resolution pattern of crossovers**

994 Crossover resolution of a dHJ from the canonical DSB repair pathway involves two
995 nicks, and two nick combinations are possible (Figure 1C). The two resolution
996 configurations can be distinguished depending on whether the D-loop invading strand
997 is cleaved or not. When the D-loop invading strand is not cleaved, the two resulting
998 hDNA tracts are in continuity with the two parental strands of the broken chromatid
999 and consist of 3' overhangs exclusively (pattern #1, Figure 1C). However, when the
1000 D-loop invading strand is cleaved, the two resulting hDNA tracts are separated from
1001 the two parental strands of the broken chromatid by a full-conversion tract (pattern
1002 #2, Figure 1C). Overall, this pattern #2 resolution is almost never observed (Table 1).

1003 Importantly, when only one hDNA tract is detected, as frequently observed,
1004 the hDNA tract is automatically in continuity with the parental strands of the broken
1005 chromatid. In this latter case, resolution pattern #1 yields a 3' overhang while pattern
1006 #2 yields a 5' overhang, which allows discrimination between the two resolution
1007 patterns (Figure S7A and B). Further complexity can arise upon HJ migration. In
1008 addition to a 3' overhang, pattern #1 can yield a 5' overhang, while pattern #2 can
1009 yield a 3' overhang in addition to a 5' overhang (Figure S7C). In such a situation, the
1010 initiating DSB is on one side of the two hDNA tracts while it is between the hDNA
1011 tracts in the canonical DSB repair pathway. These patterns do not allow
1012 discrimination between resolution pattern #1 and #2.

1013 Overall, resolution pattern #2 for one-sided events is inferred from the
1014 presence of a hDNA tract that is a 5' overhang. However, resolution pattern #1 could
1015 also formally yield a 5' overhang after HJ branch migration and when one hDNA tract
1016 is not detected as in Figure S7C. We disregarded this scenario because it is less

1017 parsimonious than the simple absence of one hDNA tract (Figure S7A), but we
1018 cannot formally exclude it.

1019

1020 **Statistical analyses**

1021 All statistical analyses were performed with the R environment ([http://www.R-](http://www.R-project.org/)
1022 [project.org/](http://www.R-project.org/)). Fisher's test, Wilcoxon's test and the exact binomial test, corresponding
1023 respectively to the R functions `fisher.test()`, `wilcox.test()`, and `binom.test()`, were
1024 always used with the two-sided option. Wilcoxon's test is applied with a continuity
1025 correction.

1026

1027 **Data availability**

1028 Octad sequences are publicly available at the NCBI Sequence Read Archive
1029 (accession number SRP111430).

1030 Sequence reads and compiled Spo11-oligo maps are publicly available at the Gene
1031 Expression Omnibus (GEO) repository (accession number GSE101339).

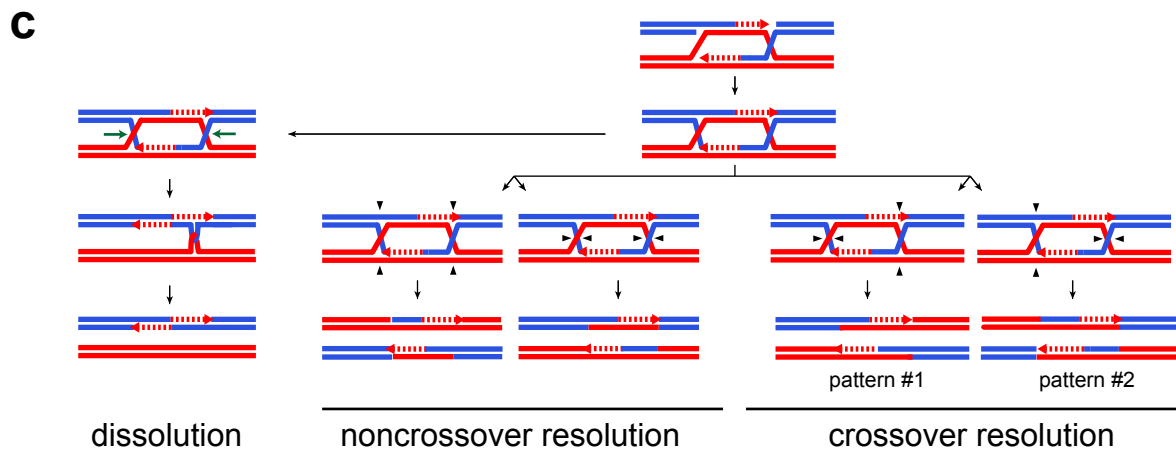
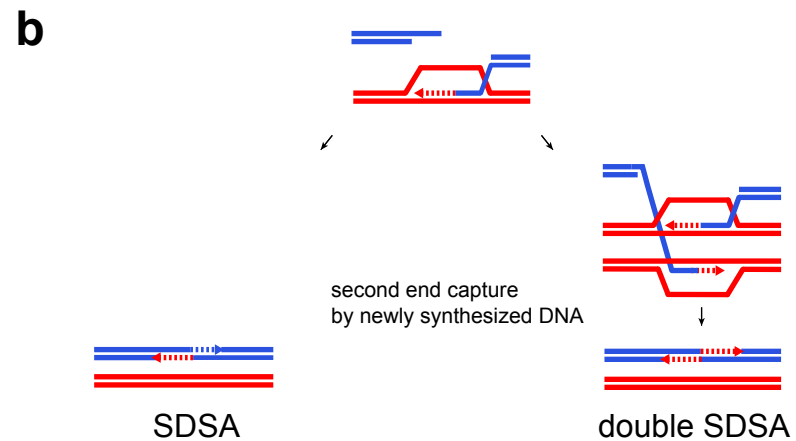
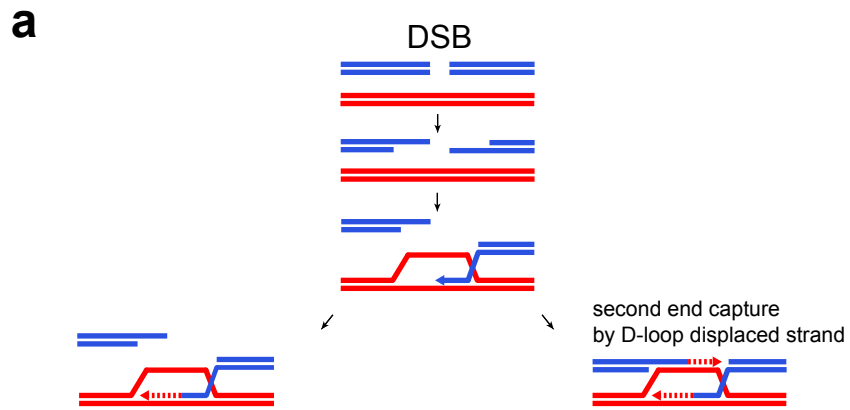


Figure 1

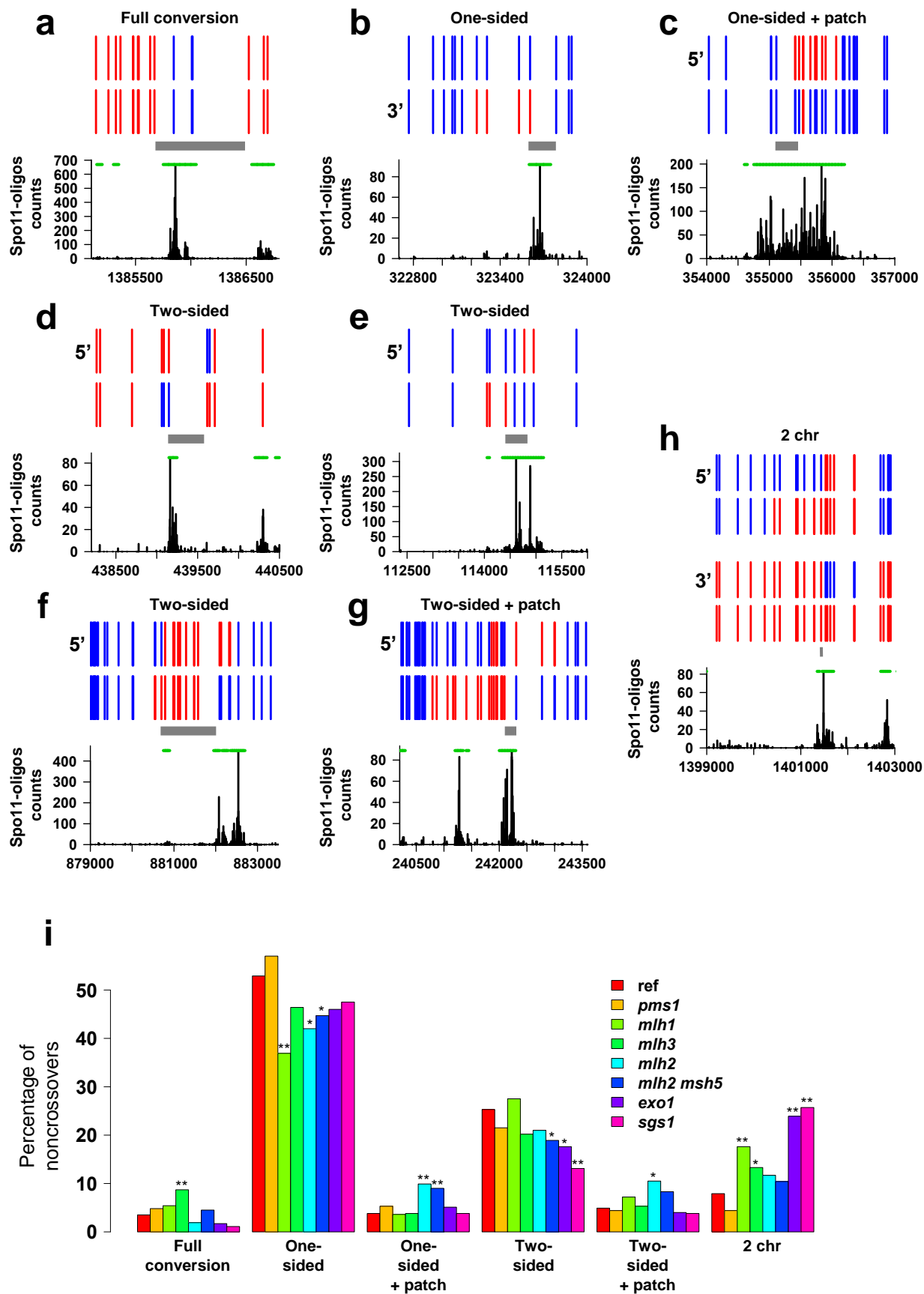


Figure 2

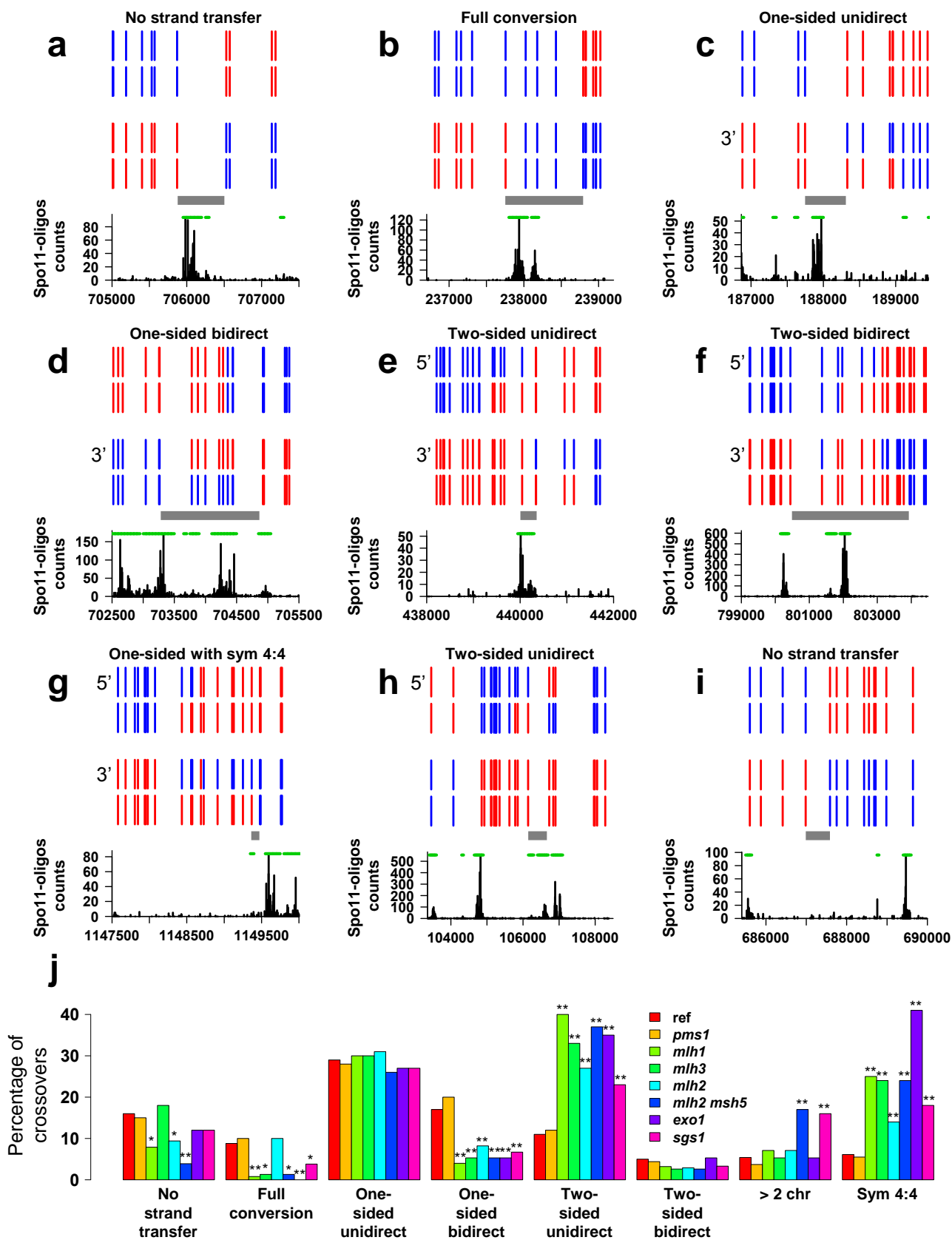
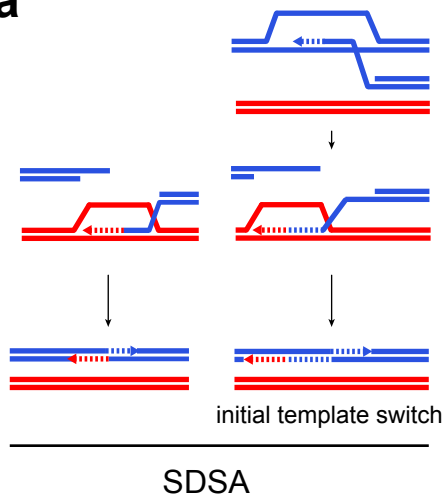
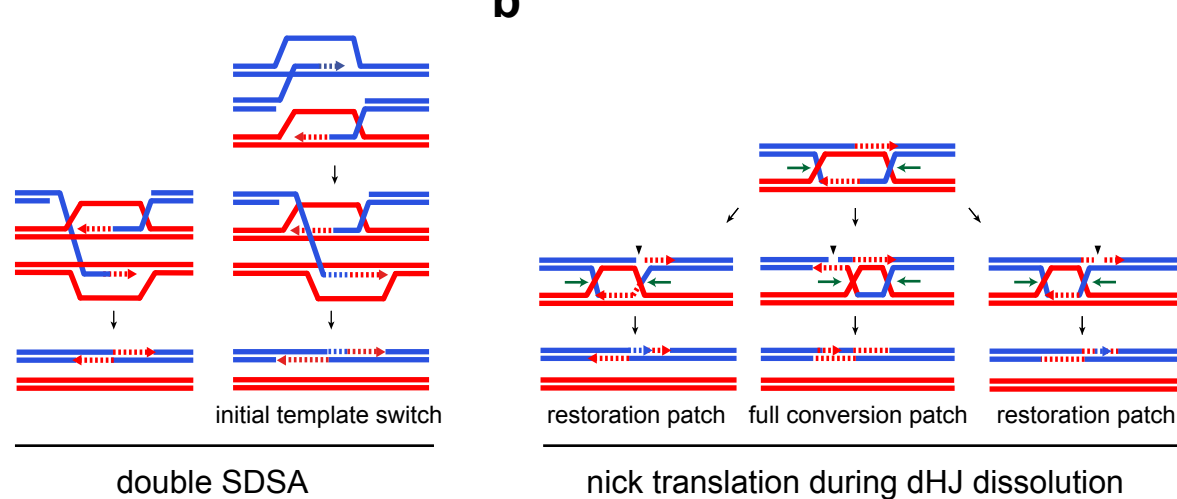
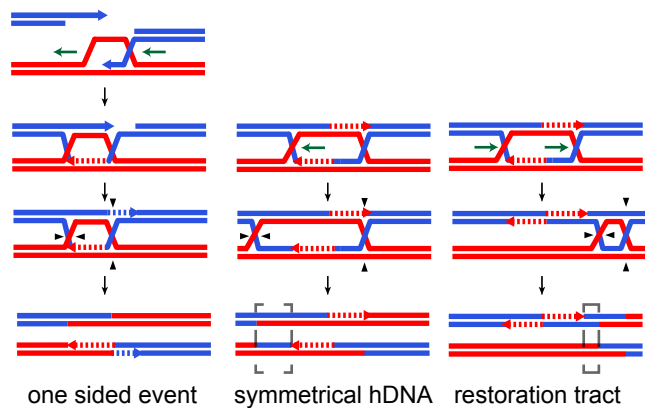
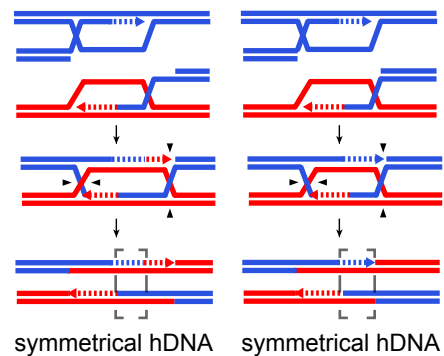
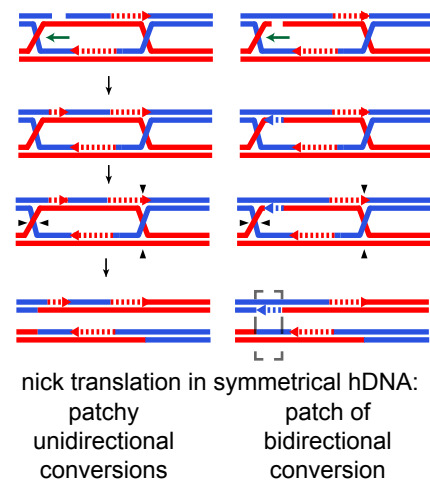


Figure 3

a**b****c****d****e**

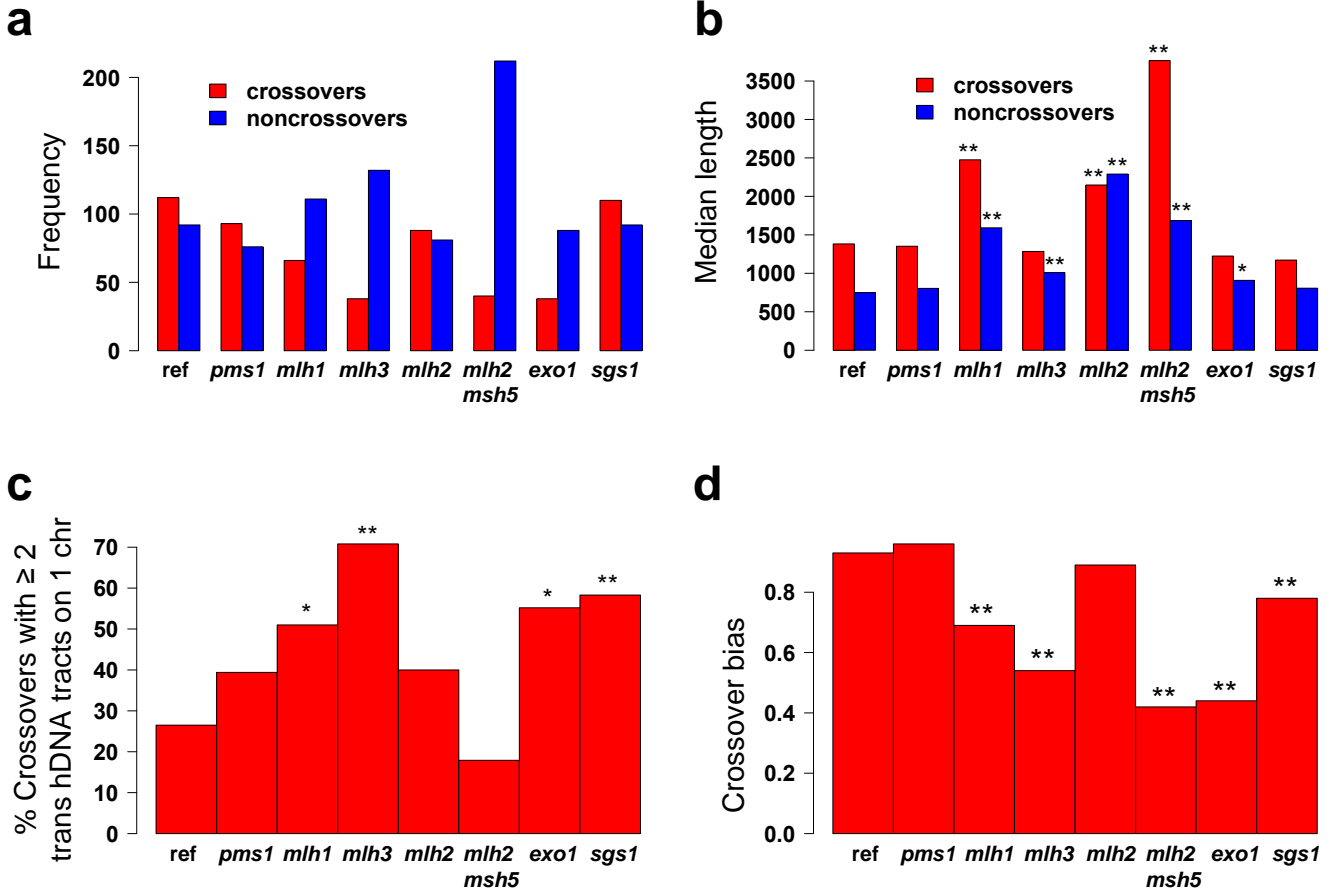


Figure 5

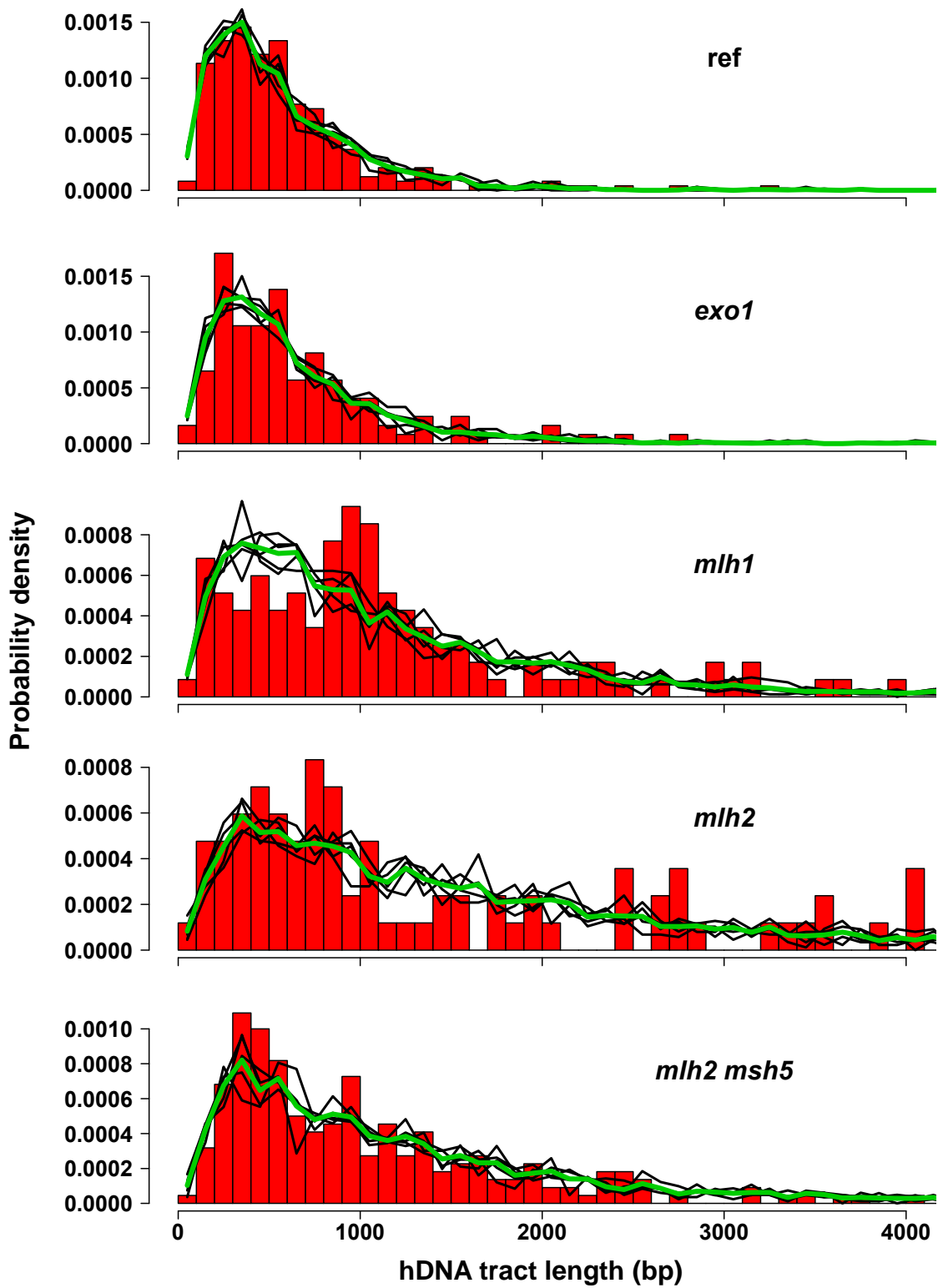


Figure 6

genotype	one-sided	one-sided	two-sided	two-sided	pvalue	pvalue	pvalue	pvalue
	pattern 1	pattern 2	pattern 1	pattern 2	1_0.5	2_0.5	1_ref	2_ref
ref	51	4	27	0	2.0×10^{-11}	1.5×10^{-8}	1.0	1.0
<i>pms1</i>	26	2	19	0	3.0×10^{-6}	3.8×10^{-6}	1.0	1.0
<i>mlh1</i>	13	7	30	1	0.26	3.0×10^{-8}	0.0061	1.0
<i>mlh3</i>	3	4	7	0	1.0	0.016	0.0037	1.0
<i>mlh2</i>	20	3	29	0	0.00049	3.7×10^{-9}	0.41	1.0
<i>mlh2 msh5</i>	6	2	19	1	0.29	4.0×10^{-5}	0.16	0.43
<i>exo1</i>	6	0	6	0	0.031	0.031	1.0	1.0
<i>sgs1</i>	15	2	20	1	0.0023	2.1×10^{-5}	0.62	0.44

Table 1. Numbers of one-sided and two-sided crossovers resolved with patterns #1 and #2. pvalue 1_0.5 and pvalue 2_0.5: *p*-values corresponding to the exact binomial test that the ratio of crossovers with pattern #2 is not statistically different from 0.5, for one-sided crossovers and for two-sided crossovers, respectively. pvalue 1_ref and pvalue 2_ref: *p*-values corresponding to Fisher's test that the ratio of crossovers with pattern #2 in the reference and in the mutant strains are not statistically different, for one-sided crossovers and for two-sided crossovers, respectively.